Proceedings of ES2009
Energy Sustainability 2009
July 19-23, 2009, San Francisco, California USA

ES2009-90163

RAPID REFLECTIVE FACET CHARACTERIZATION USING FRINGE REFLECTION TECHNIQUES

Charles E. Andraka
Scott Sadlon
Brian Myer
Kirill Trapeznikov
Christina Liebner

Sandia National Laboratories
Albuquerque, NM 87185, USA

ABSTRACT

Mirror facets for Concentrating Solar Power (CSP) systems have stringent requirements on slope accuracy in order to provide adequate system performance. This paper presents a newly developed tool that can characterize facets quickly enough for 100% inspection on a production line.

A facet for a CSP system, specifically a dish concentrator, has a parabolic design shape. This shape will concentrate near-parallel rays from the sun to a point (or a line for trough systems). Deviations of surface slope from the design shape impact the performance of the system, either losing power that misses the target, or increasing peak fluxes to undesirable levels. Three types of facet slope errors can impact performance. The first is a focal length error, typically caused by springback in the facet forming process. In this case, the wavelength of the error exceeds the size of the facet, resulting in a parabola, but with the wrong focal length. The results in a slope error that is largely systematic across the facet when the measured slope is compared to the design slope. A second shape error, in which the period of the error is on the order of the length of the facet, manifests also as a systematic slope error. In this case, the facet deviates from a parabolic shape, but can be modeled with a higher order curve. Finally, the residual errors after a model is proposed are usually lumped through a Root Mean Square (RMS) process and characterized as the 1-sigma variation of a normal distribution. This usually characterizes the small-scale imperfections in the facet, and is usually called "slope error". However, all of these deviations from design are in facet errors in the slope of the manufactured facet.

The reported characterization system, named SOFAST (Sandia Optical Fringe Analysis Slope Tool) has a computer-connected camera that images the reflective surface, which is positioned so that it views the reflection of an active target, such as an LCD screen. A series of fringe patterns are displayed on the screen while images are captured. Using the captured information, the reflected target location of each pixel of mirror viewed can be determined, and thus through a mathematical transformation, the surface normal map can be developed. This is then fitted to the selected model equation, and the errors from design are characterized. The reported system currently characterizes point focus mirrors (for dish systems), but extensions to line focus facets are planned.

While similar approaches have been explored, several key developments are presented here. The combination of the display, capture, and data reduction in one system allows rapid capture and data reduction. An "electronic boresight" approach is developed accommodating physical equipment positioning errors, making the system insensitive to setup errors. A very large number of points are determined on each facet, providing significant detail as to the location and character of the errors. The system is developed in MatLab, providing intimate interactions with the data as techniques and applications are developed. Finally, while commercial systems typically resolve the data to shape determination, this system concentrates on slope characterization and reporting, which is tailored to the solar applications.

This system can be used for facet analysis during development. However, the real payoff is in production, where complete analysis is performed in about 10 seconds. With optimized coding, this could be further reduced.

BACKGROUND

Parabolic dish systems are proposed for utility scale power generation [1] as well as distributed generation [2]. While cost is a critical component of these systems, performance cannot be sacrificed to attain low cost, without impacting the return on investment. A critical element of the performance is the reflective surface, or mirror facets. Prior study has shown that the value of the generation system is closely coupled to the quality of the reflective surface [3]. While analytical studies have been performed, a measurement tool is needed to couple the analytical studies to the practical application. In addition, the high rate of production needed to support the utility scale deployments means that either very intermittent testing is performed, or a high speed testing system must be developed to maintain 100% facet measurement. Industry-reported facet production rates are in the

range of one facet completed every 20 seconds, which means approximately 10 seconds on station would be available for full characterization.

The defacto standard for mirror characterization by the National Laboratories has been the Sandia and NREL-developed VSHOT system [4,5]. VSHOT uses a laser, reflected off the facet, and a target to characterize the location of the reflected vector. From this, the surface slope at each selected location can be calculated. Each location measured on the mirror requires repositioning the laser (through a set of controllable mirrors), and the capture of an image of the target board. Typically, 1000 to 3000 points are measured on a 1 m² facet. This data is fitted to a parabola or other representative surface shape description, and the residual difference between the local measurements and the fitted model is reported as a standard deviation of the error magnitude. The fitted model and the residual slope error provide a model of the surface suitable for analytical study. The capture of the data takes a number of minutes, limited by the laser repositioning speed and the camera capture and data transfer speed. The system reports the fitted focal length (parabolic fit) or higher order polynomial fit, as well as the residual slope error expressed as standard deviation (1-sigma) of a normal distribution of the error vector magnitudes. The VSHOT system has been extensively used in development for laboratory characterization of facet systems. The time to collect data limits the use of VSHOT for high rate production lines.

More recently, Ulmer of DLR in Germany has implemented the use of "Deflectometry" [6] to characterize facets and full dish systems. This system is being distributed and implemented on a commercial level by a spinoff company, CSP Services. Deflectometry is virtually identical to "Fringe Reflection", and is based on the same concepts that will be explored in this paper. The CSP Services Deflectometry system uses a high grade consumer camera for imaging, and a video projector for target generation. The images are manually triggered, and downloaded for post-test analysis. This system is geared toward development characterization, and is suitable for characterization of full dishes. The cited paper concerns earlier work using a colored target, which CSP Services has upgraded to the deflectometry method.

Heimsath has also presented a fringe reflection technique [7] that is in use for characterization of linear Fresnel facets. This system is geared toward the nearly-flat facets of a linear Fresnel system, and is used both in the laboratory and in the field for system characterization. The intent is in-factory quality control. The paper does not discuss the speed of the process. Heimsath has teamed with pioneers in the automotive industry's fringe reflection community. This use of fringe reflection demonstrates one approach to apply these techniques to linear focus systems.

Fringe Reflection or Deflectometry systems have been used extensively in the automotive industry to characterize surface quality of body panel and glass parts. These systems typically integrate the measured surface slopes to generate surface positional information for comparison to CAD models [8]. A significant part of the literature on these techniques concentrates on robust numerical integration techniques that can handle "real world" data with missing points in the integration field [9,10]. Another use is through differentiation of the slope information to give local curvature, which provides a very sensitive measure of surface flaws such as paint texture [11]. While we anticipate these commercial systems could be adapted to measurement of solar facets, the needs of the solar industry differ from the automotive industry, in that we are most interested in the slope data. Therefore, we chose to develop our system and software geared to support point focus (and eventually line focus) mirror characterization. In development of the software, we have discovered a number of interesting issues and application that can be exploited with direct access to the raw data and algorithms. The two cited European CSP developments reinforce the need for solar-specific algorithm and hardware development.

The fringe reflection or deflectometry systems use phase-shifted fringe patterns on a target, and view a reflection of that target in the mirror, in order to map each camera pixel image of the mirror to a specific location on the target. The process used is well documented [12]. Literally hundreds of papers cover various aspects of this topic, so only a few seminal papers are noted in this text. Once the fringe patterns are used to map a location on the mirror to a location on the target, vector algebra is used to generate the surface normal at each location on the reflective surface. The advantage of the fringe methods is that each captured set of images generates data on all points of the facet. Anywhere from 6 to 20 images may be used to characterize each point, but all points are characterized with this set of images, rather than the VSHOT method where one point is generated for each image captured.

In this paper, we present a fringe reflection technique developed in MatLab, dubbed SOFAST (Sandia Optical Fringe Analysis Slope Tool). An integrated data collection and analysis system is implemented, with the data customized for the solar application. Several proprietary facet fabrication processes had indicated a completion rate of once every 20 seconds, so we set a goal of 10 seconds dwell time to characterize the facet. We assume the facet would be placed in a fixture by a robotic handler for repeatable positioning. In addition, we develop "electronic boresighting" to analytically rotate the facet into the correct reference coordinate system for future dish system modeling. Finally, a set of captured information is identified for an archival library of facet measurements.

HARDWARE

The fringe reflection approach is shown schematically in Figure 1. A camera views the facet, which is positioned such that the camera sees the reflection of a target in the facet. The camera and target are carefully positioned relative to each other, or in our case, fastened together. The camera and target are placed near the 2-f position (twice the focal length) of the facet, so that the return signal areal extent at the target is as small as possible. A good quality facet requires a target that fits comfortably on a 24" LCD monitor. The advantage of an LCD monitor is that the spatial control of the fringe pattern and of the phase shifts is excellent [13]. The camera can be considered a pinhole, or single x,y,z position in space (C_{xyz}). Each point on the facet (F_{xyz}) can be determined through geometry and ray tracing. The pixel location (P_{xyz}) is projected through C_{xyz} and intersects with the parabolic surface to determine F_{xyz}. Finally, through the fringe analysis, the return location at the target, of each pixel can be determined. Given these three points, the incoming (**CF**) and outgoing (**FT**) vectors are determined at each point, and then the surface normal on the facet can be determined.

In setting up the system, the camera/target assembly is positioned such that all (or most) of the mirror "sees" the target from the point of view of the camera. This can be easily accomplished by displaying an all-white target, and positioning the facet while monitoring the camera image. Poorer facet quality may require a larger LCD screen to fully characterize the facet.

The use of fringe patterns to determine the return signal location is well understood [14]. Given a sinusoidal fringe brightness pattern on the target, Figure 2, and shifting that fringe 3 times, for a total of four images, one can determine the phase angle of any given pixel in the x direction, but not the absolute position in the x direction if more than one fringe period is present. The relative phase angle is determined through the formula [12]:

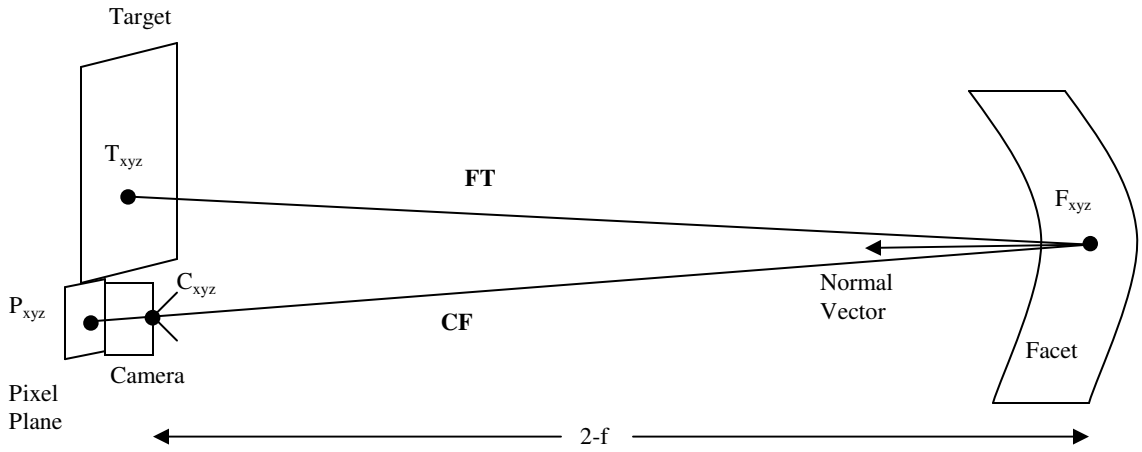

Figure 1. Schematic of SOFAST system layout. The target is an LCD screen used to display sinusoidal fringe patterns. The camera views the fringe pattern in the reflection from the facet being measured. If the point T_{xyz} can be determined, then the normal vector can be determined from vectors CF and FT.

$$\tan[\phi(x,y)] = \left[\frac{I_4 - I_2}{I_1 - I_3}\right] \qquad (1)$$

where ø is the phase angle of the target location, and the I's are the intensities of the pixel during each of the phase-shifted displays. For the example return signal indicated along the red vertical line in Figure 2, the relative phase ø is determined to be at 1.72 radians (98.3 deg) based on equation 1 with the measured brightness at each red line. In this case, since there are two periods, the result is ambiguous, as the phase of 1.72 radians occurs twice in the pattern. The process is repeated with y-direction fringes to determine the coordinates of the target position in two dimensions. Figure 3 shows the reflected view of the 4-fringe pattern in a good quality mirror.

A key feature of this approach is that the system is self-tuning, as the intensity ratios are used, rather than the absolute intensity. A number of methods are used to change this relative phase angle into an absolute angle. Most methods require a known surface slope and position at some point in the field of view, from which the absolute phase is integrated. We chose to use the "temporal phase unwrapping" method [15]. In this method, a single fringe is used first, which gives an absolute location but with a possibly significant error band. This is followed with a finer fringe pattern (more periods), such that the size of one period is larger than the error band of the prior iteration, as shown in Figure 4. The rough absolute location from the single fringe locates the return signal within a one period wide window in the finer pattern. We found that we could provide a sequence with one fringe, followed by four fringes, and get repeatability on the order of 5 pixels of the LCD target. This, at 12m distance, is roughly 0.04 mrad of surface slope uncertainty, when we are considering surfaces with residual standard deviations (RMS error) of 1-4 mrad. Other formulations in the same reference allowed as few as three patterns to find the relative phase angle, with a little less accuracy. For stability, we chose the 4 fringe method, with 1 and 4 periods, for a total of 8 images in the x direction. The process is repeated for the y direction. Our camera was suitable for 14 frames per second, but our display card took up to 0.3 seconds to complete the display of a new pattern. Therefore, the entire data collection takes about 5 seconds.

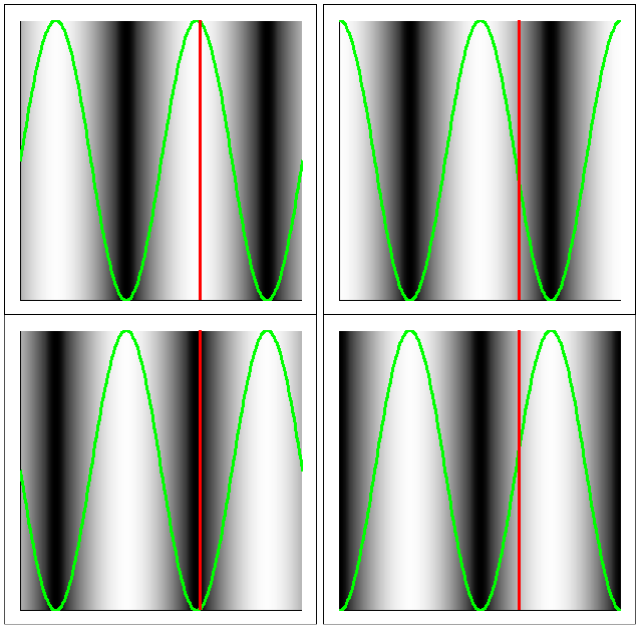

Figure 2. Fringe patterns with two periods, showing the 4 phase-shifted positions. The overlaid sinusoidal line indicates fringe brightness, and is not included on the real target. The red line indicates a sample position of the return signal. The patterns would be repeated in the horizontal direction to determine vertical position. The normalized brightnesses of the fringe at the red line are about 0.995, 0.427, 0.005, and 0.572, for phase shifts of 0, π/2, π, and 3π/2 respectively.

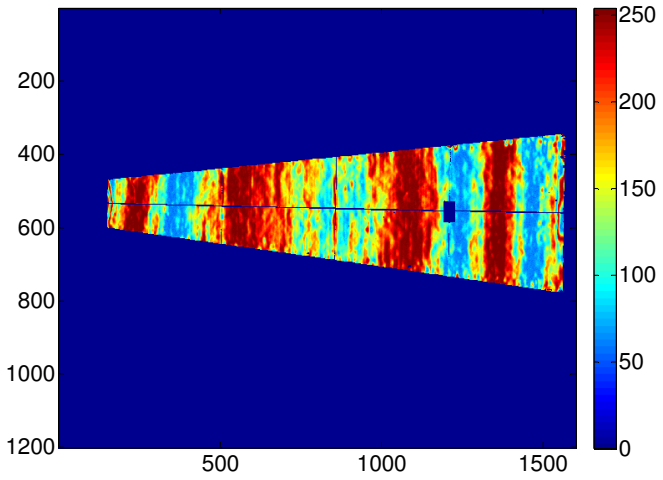

Figure 3. Reflected fringe pattern in ADDS facet. A four-fringe pattern is displayed on the target. The detected image is colorized to aid in viewing. Four such images are collected for each fringe depth, in each directions (x and y) to develop a map of the reflected image location on the LCD target. The color value is the 8-bit pixel brightness detected.

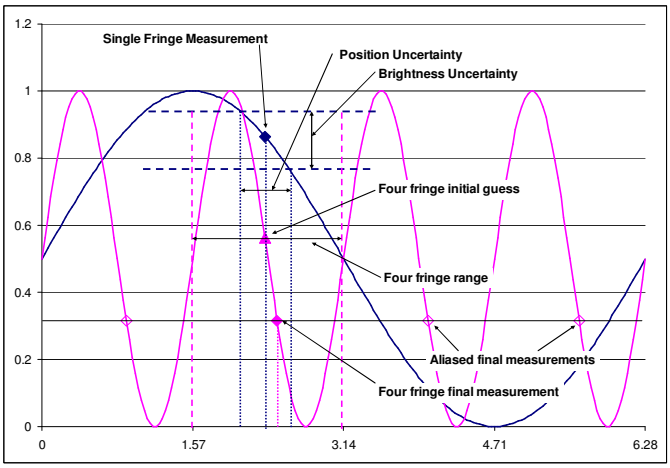

Figure 4. Temporal drill-down example. The initial measurement of phase with a single fringe locates the target signal at the blue diamond at about 2.32 radians. This measurement has a positional uncertainty based on the brightness uncertainty of the four measurements. The four fringe measurement determines the final phase, and therefore the final position, as well as three aliased positions. The positions in the four-fringe measurement are only considered within a 1-fringe window centered on the single-fringe position (four fringe initial guess), thus selecting the correct four-fringe location. The four-fringe range must be wider than the single-fringe positional uncertainty. The uncertainties shown are illustrative only.

CAMERA CALIBRATION

As engineers, we like to live in a perfect world, where a camera lens fits a pinhole model, and the camera sensor is linear with the light intensity. However, after significant measurements, we find this is not the case, even with quality equipment. Therefore, the camera needs to be characterized and the discrepancies of reality accounted for.

The first area is the lens distortions, or "intrinsic" calibration of the camera system. This is a characterization and correction of the distortions by the lens. We used a Basler 641fc firewire camera, which has a 2.1Mpix sensor (1600 x 1200 pix) [16]. We specified a Fujinon lens [17] for the initial testing. While there are substantially lower cost lenses, we found that the distortion of "security camera" grade lenses was significant. We used a canned MatLab toolbox for lens characterization [18]. A series of images of an accurate checkerboard pattern at various angles is used to develop a model of the barrel distortions of the lens, as well as the actual focal length of the lens on the camera. We found that the distortions of this series of lenses was very small. We did use the reported focal length of the lens as an input to our code. We structured the code to use the measured distortions of the lens as output from the toolbox.

The second area of calibration is the "radiometric" calibration of the system, or the response of the camera and LCD display to various commanded light levels. For flexibility we employed the color version of the camera, though in the future, with the selected implementation, a grey tone camera would be suitable. The camera response to red, green, and blue is not linearly proportional to the imaged light. Therefore, a calibration curve had to be developed. In addition, since we are imaging a reflection of an LCD screen, we also found that the LCD screen response was not linear to the programmed value. The mirror is not 100% reflective, and may have absorptivity that varies with the spectrum. We also found that too fast a shutter speed would result in a partial image as the LCD screen updated. It is therefore important to calibrate the radiometric response of the entire system, from target, through reflection, and to camera response.

The first step in the radiometric calibration is to adjust the lens aperture such that the shutter speed for full saturation is sufficiently long to avoid problems with the LCD flicker. We experimentally determined a suitable shutter speed range. We display a full white image on the screen, and then test at both ends of the acceptable shutter speed range. At the high end (long shutter speed), the image should be fully saturated. At the low end (shortest shutter speed still long enough to avoid LCD flicker) the sensor should not be saturated. This guarantees that a shutter speed in the acceptable range will provide a full range (255/255) signal for a full white (255) output on the LCD screen. Thus, the system will use the full dynamic range of the camera without saturating the camera. The optimum shutter speed within the acceptable range is determined with a simple binary search algorithm. This (and most subsequent) actions are only performed on "active" pixels. These can be determined by generating a simple binary "mask" of the image data. Two images are collected, one with a dark target and one with an all white target. The pixels that change response more than a set threshold are considered "active", as they reflect some point on the target to the camera. All non-responsive pixels are ignored.

Once the physical aperture is set, we then ramp the camera sensitivity or gain, while displaying an all-white target. This essentially varies the gain of the green receptors. We find a gain that provides an indicated average pixel brightness of about 250 (out of 255), in order to maximize the camera range without saturating pixels. We then repeat this for the red and blue "white balance", again maximizing the response without saturating. If a B&W camera is used, this only has to be done on one channel. We use a binary search algorithm to quickly find the gain that provides a response of 250.

Finally, we need to map the end-to-end response of the system (LCD, reflection, and camera). We ramp a uniform image on the LCD from 0 to 255 while recording the average response of the active

pixels. We find the response somewhat flat at low brightness, which makes the low end of image display brightness of limited value. We determine the commanded brightness at which the change in camera response is positive with a positive stimulus, and use this as a "floor". We also look for saturation at the bright end, though this should not happen since we already set the gain of the system. We fit a 7^{th} order polynomial to the camera response, which we use later to scale the fringe pattern brightness, thus linearizing the system from commanded stimulus to sensed brightness. This could be performed at a pixel level, but such calibration would then have to be performed for each facet. We found with good quality LCD screens that the response across the screen was sufficiently uniform. We perform the radiometric calibrations once per day, or when we determine there has been a significant change in room lighting. The camera must be warmed up at least half an hour before calibration for the most consistent results.

The third area of calibration is the position of the camera, target, and facet relative to each other. We carefully measure the fixture that holds the camera relative to the target. We have design information on the facet, which allows us to use a single camera observation to determine the camera location relative to the facet in 6 degrees of freedom. We use the extrinsic analysis portion of the Camera Calibration Toolkit [18] to perform this analysis. Given the real-world coordinates of the corners of the facet, we are able to determine the camera location in the facet coordinate system within a few centimeters as an initial guess on position. This is refined later in the analysis section. We also make a distance measurement from the center of the target screen to a selected location on the facet. We perform this measurement with a Disto [19] laser range finder, accurate to 3mm. We use this physical measurement in the later refinement of the camera position. Several standard edge detection methods are used to locate the physical corners of the reflective surface. This task is simplified by using the mask rather than the raw image, which provides very definite edges of the facet. Figure 5 shows the mask and the located corners for an ADDS [20] parabolic facet. The edge lines are located, and the intersections determine the four corner points, labeled 1 through 4. Additional feature points are located by projection once the coordinate system is determined. In this case, the reference points are splits between separate pieces of glass on the facet, and make handy reference locations for the Disto measurements.

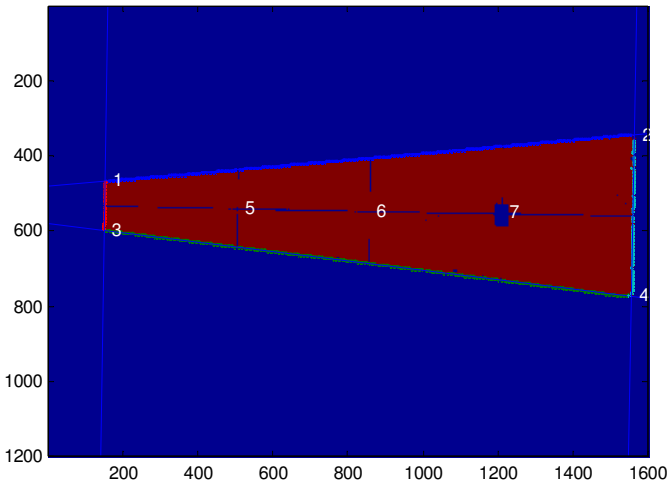

Figure 5. Active pixel mask and located edges and corners. The large inactive area at point 7 is a "yellow sticky" on the facet used temporarily for measurements. Points 1 through 4 are the located corners, and points 5 through 7 are key locations on the facet for reference. In this case, the key locations are at splits between the subfacet pieces of glass, which make a handy reference.

DATA COLLECTION

The fringe patterns are scaled to fill the LCD screen. The sinusoidal brightness variation goes from the floor to the maximum as determined in the radiometric calibration, and is linearized by the system response curve. The first set of fringe patterns displayed contain a single period, which gives an absolute screen location. Each point measured on the mirror is independent of neighboring points, making this method suitable for "difficult" mirrors (very distorted). Methods of characterization that rely on fixed line patterns or shape keys on a target require "coherent" images, where the shape of the line or key can be recognized in the reflected image. Each brightness measurement has a range of uncertainty, which leads to uncertainty in the position determination. This can then be refined with more periods, as long as the length of a single period on the screen exceeds the uncertainty band of the prior fringe measurement. Through trial and error, we saw little improvement beyond 4 periods on the target, and found that we can robustly transition from 1 to 4 periods (meaning the width of one period in the 4-fringe pattern was significantly wider than the error band of the single fringe, so the correct period was routinely captured in the four-fringe run). We also found the refinement in going to 4 periods was usually less than 10 pixels, so it would be feasible to only record the single-period data. However, we still use the 4-period data to refine our results. However, when larger LCD targets or projection screens are used for less accurate facets or full dishes, this refinement is likely more important than in these tests.

We experimented with using a single grayscale gradient (linear) on the screen for the initial absolute location estimate. This approach is not self-calibrating for brightness of the signal. In many cases we found we could go from the single linear gradient to the four periods robustly, and get the same results as the full fringe periods. However, the savings is limited to 3 images in each direction, and we determined that adding the uncertainty imposed by potentially changing lighting conditions outweighed the time savings for this implementation of the tool.

The collected fringe data can be saved in a "Data dump". This is helpful in development, as we can re-analyze the collected data should the characterization algorithms be improved. This is the equivalent of saving raw voltage data rather than the engineering units in a data acquisition system.

DATA REDUCTION

The reflected target location information for each point on the mirror is reduced in an interative process to determine the surface normal (slope) at each point on the facet surface. In iterative process is needed because the measured shape of the facet may differ form the design shape, and must be integrated from the slope data. However, the slope data depends upon the facet shape. The basic fitting process follows these steps, and is detailed after:

1. Determine the initial assumed coordinates of the camera and target in the facet coordinate system, using extrinsic analysis combined with the Disto measurement from the target to a point on the facet.
2. Select a "design" facet shape model , typically a simple parabola of rotation.
3. Project each camera pixel on the pixel plane (P in figure 1), through the center of the lens (camera location, C in figure 1), and intersect with the facet shape model. If the shape

model is parabolic, this involves solving a quadtratic equation for each camera pixel. This process provides the x,y,z coordinates of the pixel ray intersection with the facet, point F in figure 1.

4. Using the camera location (C in figure 1), facet point location (F), and the measured target point (T) for each viewed point on the facet (corresponding to each pixel in the camera image), determine the surface normal at each point
5. Fit the surface slopes at each point to the partial derivatives of the model shape equation, using a least squares fit. This gives coefficients of the derivative equations, and therefore coefficients of the model shape equation. Adjust the constant term of the model shape such that the Disto measured distance remains fixed.
6. Repeat steps 3 through 5 using the new fitted shape equation. Repeat until the solution converges. This appears quick, typically 3 iterations is enough.
7. Adjust coordinate system such that the fitted position and normal at the "alignment point" (a selected point on the facet that will represent the entire facet for alignment purposes) matches the design facet position and normal. Repeat steps 3 through 7 until solution converges, typically 3-4 iterations. This places the facet information in a useful and consistent coordinate system for further analysis.

We selected a 3-D parabolic equation in Cartesian coordinates for our primary facet shape model, based on the published VSHOT approach [4]. This equation allows a different focal length in the X and Y directions, which can occur in imperfect manufacturing processes of point focus mirrors, and in the design case of line focus mirrors. The parabolic model is expressed as:

$$z=Ax^2+By^2+Cx+Dy+Exy+F \quad (2)$$

Step 4 in the process converts the collected target data into a surface normal at each location on the facet, which can easily be expressed as a slope in the x and y directions at each location. It is these slopes that are fitted, so we fit the data to the partial derivatives of the model equation:

The first step in the data reduction is the determination of the normal vector at each location on the mirror. In order to attain this information, we need the location of the camera (pinhole model), the target (target pixel as measured), and the point on the facet. As noted earlier, we know the position of the camera and target relative to the facet coordinate system through an extrinsic analysis of the mirror corners in the captured image mask, as well as the relative positions of the camera and target. We also can model the position of each pixel on the sensor plane, relative to the lens pinhole model, by developing this plane and performing the camera position rotations and translations. The location of the camera pinhole and each pixel provides a vector for each pixel, going from the camera to the facet. We only know that the data sensed by each pixel is on this vector, but we do not know the length of the vector. However, we can model the facet, and determine the intersection of the vector with the facet surface. If the facet model is parabolic, then the intersect location can be determined through a quadratic equation. However, if the model is a higher order, one must use an iterative process to locate the intersect of the vector with the facet.

$$\frac{\partial z}{\partial x} = 2Ax + C + Ey \quad (3)$$

$$\frac{\partial z}{\partial y} = 2By + D + Ex \quad (4)$$

A simple least squares linear fit of the data to equations 3 and 4 is performed. The linear terms of the model spatial equation (C and D in (2)) become fixed slopes in the slope equations, and thus can be interpreted as a tilt (constant additional slope), at least for small tilts. However, it can also be interpreted in the model shape equation as a diagonal spatial translation of the origin of the parabola. The effect is the same for small tilts. The cross term, Exy, can be interpreted in the model equation as a rotation of the principle axes (greatest and smallest focal lengths) of an elliptical 3-D parabola relative to the physical orientation of the measured facet. However, in slope space, one can see that a tilt is added in equation 3 in the x direction, which increases as y increases. This term, thus, can also be interpreted as a twist. This interpretation has little value if a full parabola of rotation (or elliptical parabola) is considered, but we generally consider a narrow slice of the parabola, such as the ADDS gore facets. If the facets are well made, this term should approach 0. However, we have seen on some high aspect ratio facets that the twist can be significant, and that the twist term is not equal in each fitted partial derivative. Most texts that deal with this model equation consider full circular or elliptical shapes, and so this twist interpretation is not typically made.

The fitting process is a standard least squares fit to the two linear equations. The coefficients are then assembled into the model shape equation. The constant term, F, is adjusted such that the measured distance to a single point on the facet is maintained. When assembling the partial derivatives into the model shape equation, the E term is averaged.

The fitted model shape equation will likely differ from the initial (design) model equation. This new shape will change the intersections of the camera pixel rays (**CF**) with the facet (point F), and therefore the surface normal will slightly change. Thus, the process is iterated until the shape and slope cease to substantially change. During the initial fitting, we only use 10% of the facet points (camera pixels), in order to substantially speed up the fitting process. A typical facet has 400,000 to 700,000 pixels active on our 2.1 Mpix camera, and so we are fitting to at least 40,000 points. Once the fit has converged, we perform a final fit with all of the datapoints.

It is important to select a coordinate system that suits the facets naturally, as well as is supported by the analysis tools used for post-processing. For small spherical facets that simulate a parabola through the use of many facets, we designate the physical middle of the facet as the origin, and the x axis is typically along the longer dimension. This is typical of the McDonnell Douglass [21] and Stirling Energy Systems [22] dishes. A parabolic gore facet is a segment of a parabola of rotation, and has the natural origin at the vertex of the parabola. The z axis is the axis of rotation (were the facet to have the same focal length in x and y), and the x-y plane perpendicular. The x axis is aligned with the projection of the centerline of the gore onto the x-y plane. See Figure 6 for sample coordinate systems. It is important to note that the origin on a typical gore facet is not even on the physical facet, which adds to the difficulty in setup and interpretation.

We also can perform a fit to a higher order 3-D polynomial curve, in order to more closely model the shape of an imperfect facet. This fitting is performed after a parabolic fit session is completed. The higher order curve has proportionally more cross terms, which we do not attempt to interpret at this point.

The coordinate system for the facet is in part determined by the assumed location of the camera and target, which was initially determined by the extrinsic analysis of the corner locations. Error in

this location will lead to tilt of the facet relative to the assumed coordinate system. In VSHOT, if the linear (tilt) terms in z space are not "small", then the physical arrangement is changed and the process is repeated. However, in our system, as long as the camera can "see" the target in every part of the facet, then we only have to change the assumed location of the camera and recalculate the normals, in effect moving the coordinate system to line up with the facet. Initially we performed this step by adjusting the numerical values of the camera location and tilt proportionally to the tilt terms. We also adjust the constant term in the parabolic equation such that the laser distance finder measurement matches. In effect, this process makes the origin of the facet lie at 0,0,0 of the assumed coordinate system, and the surface normal at the origin is 0,0,1. This is usually appropriate for small spherical facets, where the origin is at the center of the physical facet. However, on the large, slender gore facets, this location is not even on the facet. If one measured a focal length error, but set the vertex normal vector to 0,0,1, then the tilt and z position of the actual facet at the radii of interest will deviate substantially from design, as shown in 2 dimensions in Figure 7. In addition, if there is a twist in the facet, the model coordinate system can be tilted substantially off the reflection of the physical facet.

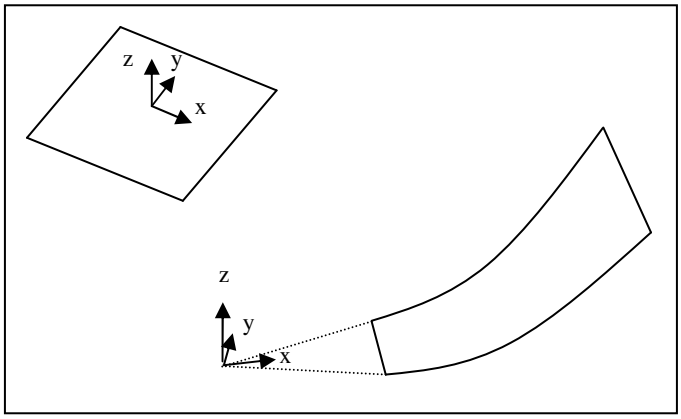

Figure 6. Typical Facet Coordinate Systems (FCS) for spherical and gore facets. The origin of gore facets is not on the physical facet.

We therefore determined that a point on the facet should be used to "anchor" the coordinate system to match the design facet. In effect, when a dish is physically aligned in the field, the facets are positioned such that some point on the facet matches the design position, and the facet is rotated such that the surface normal at that location matches the design facet surface normal. If the facet were perfect, every point on the facet would match the design. However, on a facet with shape and slope imperfections, one point is selected to represent the entire facet. We typically select a point near the outer end of the facet for this "perfect alignment" point [23], and the rest of the facet is allowed to "float". We implement such a process as follows:

1. The x,y,z position of the fitted facet shape at the alignment point is set to the design spatial position. This is effected by calculating the fitted model facet shape z position at the design x,y position of the alignment point, and then setting the constant term (F) so that the z position matches design.
2. An analytical sphere is developed about the point at which we made a physical distance measurement (Disto point). This does NOT have to be the same as the alignment point. This is the distance to the center of the target, which is used for a reference in our measurement tool.
3. The design normal vector at the alignment point is projected to the sphere. This intersection is the new location of the camera/target assembly. This places the camera/target assembly at the measured distance from the Disto point on the facet, and also places it along the *design normal vector*
4. The *fitted normal vector* at the alignment point is intersected with the target plane, which determines the measured camera position in the coordinate system under which the measurements are made
5. The camera array is translated and rotated such that it lies on the design location found in (3), and such that the pixel vector for the alignment point intersects the fitted facet shape at the alignment point

This process results in a facet coordinate system in which the fitted facet shape is tilted and positioned such that the physical alignment point matches the design alignment point in 6 degrees of freedom, and the distance to the camera is set by the physical measurement. This results in the facet being oriented in the dish coordinate system analytically the same way it will be oriented physically when the dish is aligned. This also results in appropriate tilt terms in the fitted equation.

The change in the coordinate system also requires iteration, repeating the facet normal calculations. We implement two nested loops. The coordinate system is re-calculated after three loops of surface shape modifications. This whole process repeats three times to get a stable facet shape and coordinate system. The full-resolution calculation is only performed after all iterations, and we typically do

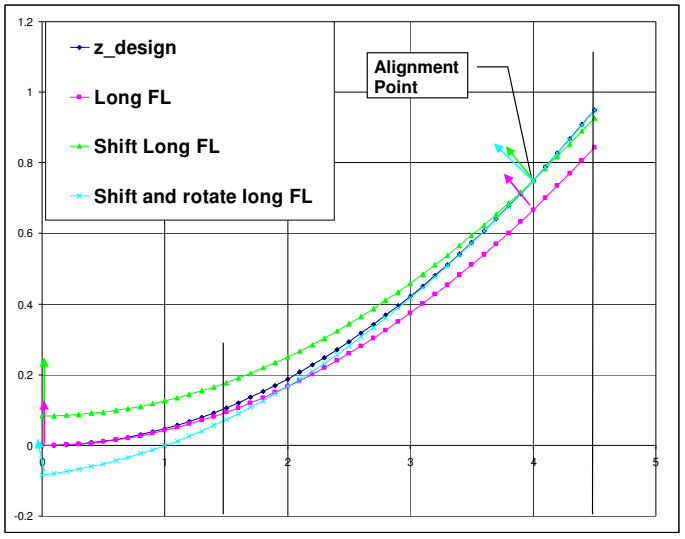

Figure 7. Parabolic fitting when the focal length is not correct. In this case, the facet extends from 1.5 to 4.5 meters. The design curve has the correct slope and position at each location. The long focal length matches the design curve slope and position at the origin, but matches neither at the alignment point. The shifted long focal length matches the slope at the origin, but matches the position at the alignment point, selected at 4 m. Finally, the rotated and shifted long focal length matches the design facet in position and slope at the alignment point (4 m), and neither match at the origin.

not see a change in measured parameters when going to all the points.

At this point, a final run may be added, in which the slope fitting is to a higher order curve than linear. For this process, we use the fitted parabolic facet model shape to determine the x,y,z coordinates of each pixel view vector with the surface. We assume that only very small changes from the parabolic fit would be present in a reasonable facet, and thus we avoid the nonlinear iterative process that would have to be used to find the intersects with a higher order shape.

We now have three models of the facet shape and slopes: the design shape model, the fitted parabola, and the fitted higher order curve. We also have the measured surface normal at each location. The difference between the measured values and the surface models is a residual slope error. While many seem to characterize a facet quality with a single "slope error" number, we find that slope error must be combined with a surface model, and it represents those measured features that are not captured by the surface model. We "model" the residual as a normally distributed error, and we report the standard deviation as an "RMS", or Root Mean Square error. It is a simple matter to calculate the slope error (in radians, not in slope units) at each measured location by comparing the measured value to the model value. The resulting slope errors, combined with focal length and other shape deviations from design, can be used to provide a figure of merit for the facet. If the models represent a reasonable fit to the facet (i.e., the residual is distributed), the model equations and normally-distributed residual can be used to model the facet system. If a reasonable fit to a model cannot be found, the large number of actual slope measurements can be used in a ray trace program to fully model the facet system.

RESULTS

In an example, high quality facet, we characterized a gore facet from the ADDS dish [20] at Sandia National Laboratories. Figure 8 shows the resulting comparison to the design facet shape. The image color is proportional to the magnitude of the error vector at every pixel. The white quiver arrows indicate direction and magnitude of the error at every tenth point, so as not to crowd the image. The total residual slope error (magnitude of the resultant vector) is 1.5 mrad. However, we see the x direction error is 1.4 mrad, while the y direction is only 0.5 mrad. We also see that the alignment point is along the centerline, ¾ of the way out on the facet, where the slope error approaches 0 mrad. Finally, we see that the slope error is very systematic in the x direction, indicating the model does not well represent the surface shape, likely due to a focal length error. In this case, reporting a residual slope error of 1.5 mrad from the design condition, as a standard deviation, does not adequately model the shape of the facet.

In Figure 9, we compare the measured slope to the parabolic fit shape model derived from the measured data, and the residual is lowered substantially, to a resultant magnitude standard deviation of 0.78 mrad, with 0.48 mrad in the y direction and only 0.62 mrad in the x direction. The fitted focal length is 5.42 m in the x direction, and 5.35 m in the y direction, compared to the design focal length of 5.33 m. The residual is far less systematic, and therefore does a reasonable job capturing the errors not modeled. Note also that twist of the facet is reported, though it is very small in this facet, at 0.1 to 0.15 mrad/m. This facet would be reported with the measured focal lengths and twist, with a residual slope error of 0.78 mrad. We do note, however, some systematic vectors of error at the left end and the center of the facet. These are shape errors that are not captured by the parabolic fit, but are more systematic than the assumed normal distribution.

Finally, Figure 10 shows the residual slope error when fitted to a 3rd-order shape model. The systematic areas of error are gone, and the primary error is seen as striations in the glass, and minor damage along the edges of the facet from handling. The resultant magnitude residual now has a standard deviation of 0.63 mrad, with both the x and y components about 0.4 to 0.5 mrad. This facet could be reported with the complete 3rd-order shape model equation plus this residual slope error. This residual is also a representation of the potential of this fabrication technique. If one assumes that gross shape errors can be corrected, then this comparison to a higher order shape model would indicate the residual one could attain compared to the design shape if process modifications address shape errors.

In Figure 11 and Figure 12, we compare the results of SOFAST with an identical facet tested with the VSHOT system. This facet clearly shows "print through" of the three mounts, one top and bottom about 1/3 from the left, and one centered vertically about ¾ from the left. While the error is locally systematic, it is also somewhat spread about the facet, and a random distribution may not be too bad an approximation. Higher order polynomial fits did not improve the shape

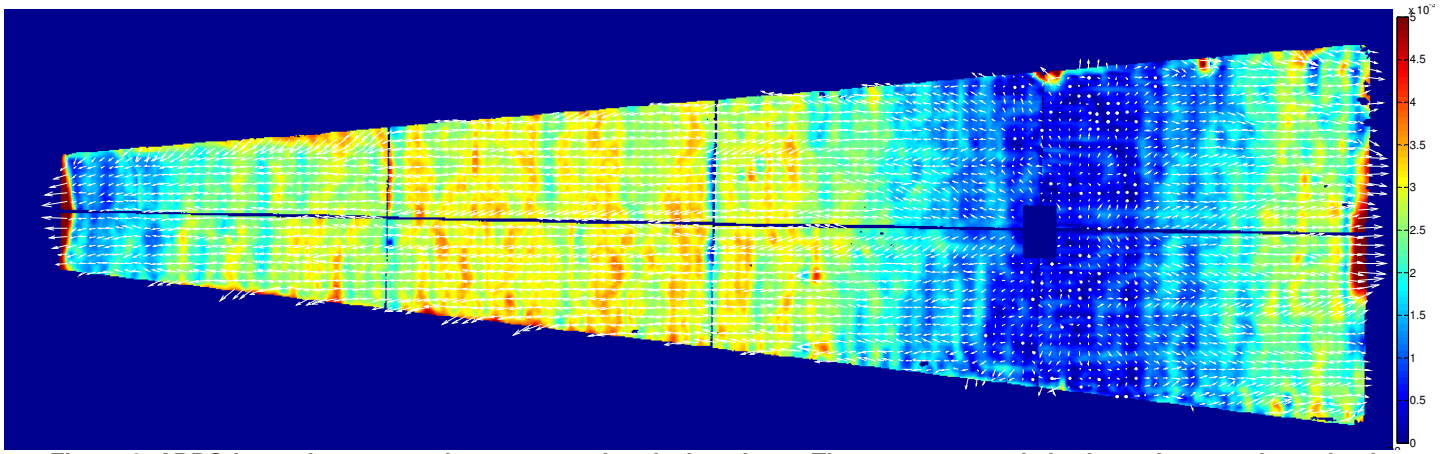

Figure 8. ADDS facet slope error when compared to design shape. The very systematic horizontal errors shown by the vectors indicate a focal length error. The pixel color indicates the total slope error compared to the design slope, while the white arrows indicate the direction and magnitude of the error at every 10th pixel (the shortest arrow appear as dots). The residual slope error standard deviation of magnitude is 2.31 mrad, with 2.25 mrad in the x direction and 0.53 mrad in the y direction. The color scale ranges from 0 mrad (blue) to 5 mrad (maroon).

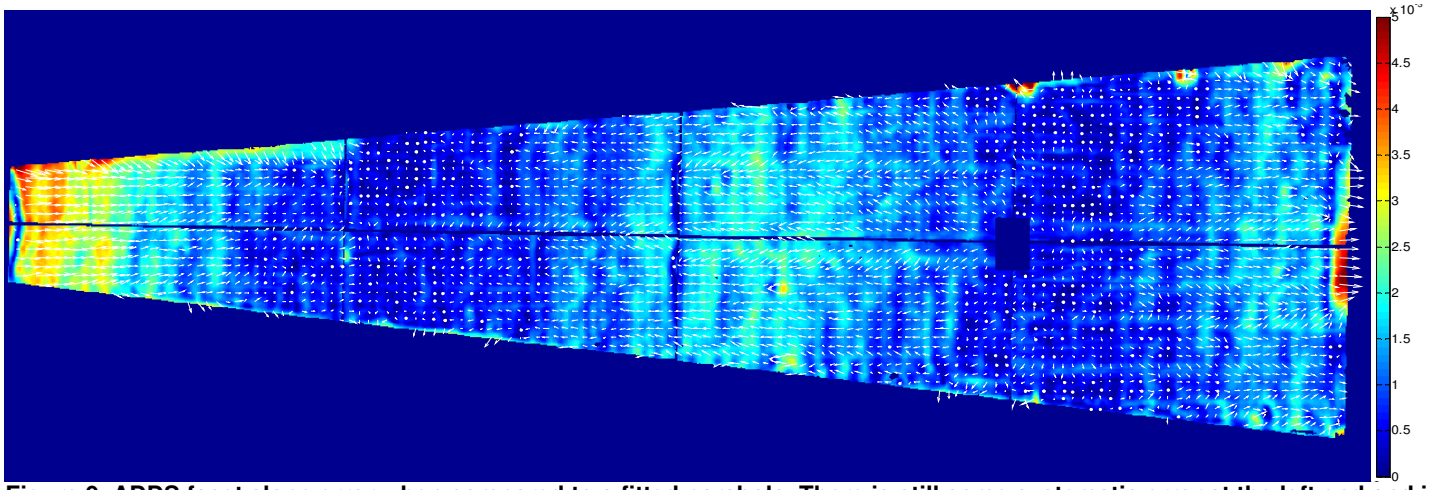

Figure 9. ADDS facet slope error when compared to a fitted parabola. There is still some systematic error at the left end and in the center, indicating that the parabolic fit may not completely model the surface shape. The residual slope error magnitude is indicated by pixel color, and the direction and magnitude of the residual is indicated by the white arrows at every 10th pixel. The residual slope error standard deviation of magnitude is 1.35 mrad. Same scaling as figure 8.

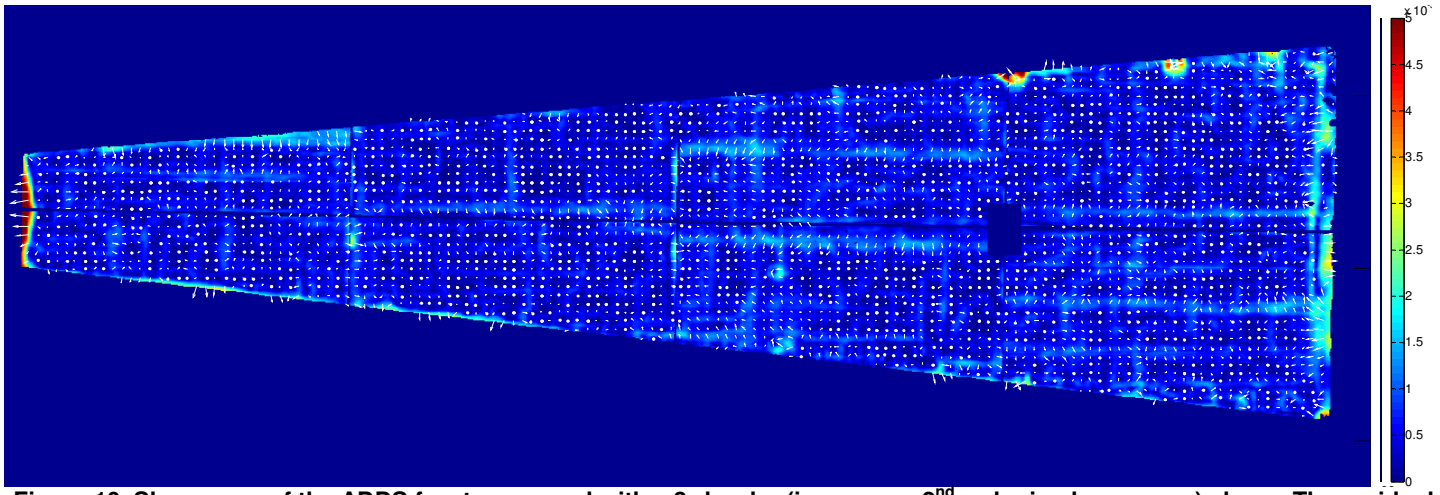

Figure 10. Slope error of the ADDS facet compared with a 3rd order (in z space, 2nd order in slope space) shape. The residual slope error appears mostly random, indicating this model fits the facet. The residual slope error standard deviation of magnitude is 0.70 mrad. The color scaling is again 0 to 5 mrad, blue to maroon.

descriptor very much, because the shape errors are localized an no global shape model was found that captured these local shape errors . The focal length measurement matches well between the VSHOT data and the SOFAST data, as does the total residual of 1.5 mrad.

After characterization, the SOFAST system adds a description line to an excel file, so that facets can be archived by serial number. We save the calculated focal lengths, the residuals compared to each model, the fitted parabolic model, the camera settings, the measured distance, and the date, time, and serial number. This results in a fairly complete database of facet quality that can be stored in company archives. In addition, on command we can store the images shown here, as well as a full "data dump" that would allow complete reconstruction of each test. The data dump is 6-8 MB in size, so it may not be practical to store such data on every facet, but perhaps on occasional facets in a systematic sequence.

While a full error and uncertainty characterization will be performed at a later date, we did explore some of the error and repeatability capabilities of this system. We identified the distance between the target/camera and the facet surface to be the measured item with the greatest uncertainty. We therefore explored the response of the system to a range of input "measured" distance without changing the camera location. Within a few 10's of centimeters of the actual measured position, we found that errors in the distance measurement had very little effect on the residual slope error results. However, we did find that for every centimeter of change in the entered distance, with the same collected data, the resultant focal length changed by about ½ cm. Second, without changing anything in the physical setup, we repeated a full measurement several times sequentially, and found that the measured return location on the target screen varied up to about 5 pixels. The pixel pitch on the monitor was 0.25mm, so the variation in measurement was 1.25 mm. At 12 m distance, with a reflected ray (law of reflection doubles the tilt), this corresponds to a repeatability of about 0.05 mrad for each point, far smaller than the range we are interested in. A complete analysis of the standard deviation of the repeatability should be performed.

SUMMARY

A tool has been developed that fully characterizes point focus solar mirror facets at a rate suitable for production line archive testing

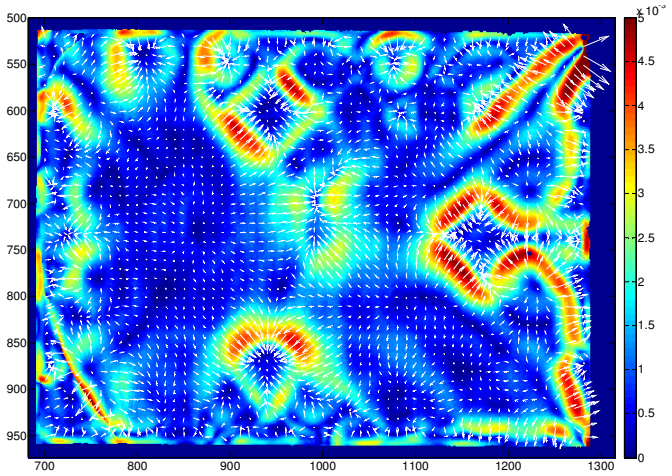

Figure 11. Slope error of MDAC "Egg Crate" facet compared to parabolic fit, as determined with SOFAST. Note the print-through of the three mounts. The standard deviation of the residual is 1.5 mrad. The color indicates the total slope error at each pixel, while the white arrows indicate the direction of the error at every 10th pixel. The slope is measured at over 264,000 points on the facet.

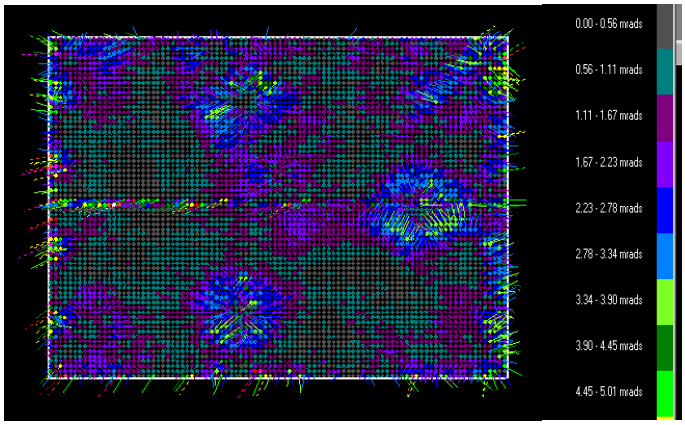

Figure 12. Slope error of the same MDAC "Egg Crate" facet as determined by VSHOT. The standard deviation of the residual is 1.64 mrad. The slope is measured at 6580 points on the facet. Image courtesy of Tim Wendelin, NREL.

of 100% of the manufactured facets. The approach taken couples the camera data directly into the target control and data reduction systems, and thus eliminates time-consuming post-processing. A key feature is the "electronic boresighting", which appropriately positions the coordinate system around the facet such that the facet fitted shape is suitable for analysis in design codes such as Sandia's CIRCE2 [24]. In addition, we have introduced further understanding of the shape errors detected with the fitting process, including twist of the facet. This is important for high aspect ratio facets such as the ADDS shown in this report.

The measurements from this system compare favorably with prior tools such as VSHOT. The tool has proven useful in the development of commercial grade facets for deployment on the SES systems, as it provides very fast feedback to engineers in the product refinement process.

In future work, we will combine this tool more directly with CIRCE2 modeling tools. Rather than introducing the analytical fitted model to CIRCE2, we will import the surface normals and locations directly into CIRCE2, and model the reflected energy from a set of measured facets. With the large number of points per facet, this will provide unprecedented fidelity in the modeling process. In addition, we would like to fully characterize the measurement error sensitivities on this process, as has been done with VSHOT[5]. The optics and geometry are similar, so the VSHOT analysis of error is mostly applicable, but should be repeated for this new tool.

ACKNOWLEDGEMENTS

This manuscript has been authored by Sandia Corporation under Contract No. DE-AC04-94AL85000 with the U.S. Department of Energy. The United States Government retains and the publisher, by accepting the article for publication, acknowledges that the United States Government retains a non-exclusive, paid-up, irrevocable, world-wide license to publish or reproduce the published form of this manuscript, or allow others to do so, for United States Government purposes.

REFERENCES

[1] Liden, R., 2007, "Solar Dish Stirling Systems Report", *NREL CSP Technology Workshop,* Denver, CO, March.

[2] 2003, "Solar Energy Technologies Program Multi-Year Technical Plan 2003-2007 and beyond", U.S. Department of Energy, Energy Efficiency and Renewable Energy, DOE/GO-102004-1775, Washington, DC, January 2004.

[3] Andraka, C.E., "Cost/Performance Tradeoffs for Reflectors Used in Solar Concentrating Dish Systems", Proceedings of ES2008, Energy Sustainability 2008 conference, ES2008-54048, Jacksonville, FL, August 10-14, 2008.

[4] Jones, S.A, Neal, D.R., Gruetzner, J.K., Houser, R.M., Edgar, R.M., Kent, J., Wendelin, T.J., 1996, "VSHOT: A Tool for Characterizing Large, Imprecise Reflectors", *International Symposium on Optical Science Engineering and Instrumentation,* Denver, CO.

[5] Jones, S. A.; Gruetzner, J. K.; Houser, R. M.; Edgar, R. M.; Wendelin, T. J., 1997, "VSHOT Measurement Uncertainty and Experimental Sensitivity Study". *IECEC-97: Proceedings of the Thirty-Second Intersociety Energy Conversion Engineering Conference, 27 July - 1 August 1997, Honolulu, Hawaii. Volume 3: Energy Systems, Renewable Energy Resources, Environmental Impact and Policy Impacts on Energy,* American Institute of Chemical Engineers, New York, NY, **vol 3,** pp. 1877-1882.

[6] Ulmer, S., Heller, P., Reinalter, W., 2008, „Slope Measurements of Parabolic Dish Concentrators Using Color-Coded Targets", *Journal of Solar Energy Engineering,*Vol 130, Transactions of the ASME #011015.

[7] Heimsath, A., Platzer, W., Bothe, T., Wansong, L., 2008, "Characterization of Optical Components for Linear Fresnel Collectors by Fringe Reflection Method", *Proceedings of Solar Paces Conference*, Las Vegas, NV.

[8] *Sensors automate reflective quality control,* Engineering Talk Website, www.engineeringtalk.com/news/mip/mip140.html, November 16, 2007

[9] Li, W., Bothe, T., von Kopylow, C., Jüptner, W., "Evaluation Methods for Gradient Measurement Techniques", *Optical*

Metrology in Production Engineering, Proceedings of SPIE Vol. 5457, Bellingham WA.

[10] Agrawal, A., Raskar, R., Chellappa, R., "What is the Range of Surface Reconstructions from a Gradient Field", Proc. European Conf. Computer Vision, May 2006.

[11] Höfling, R., Aswendt, P., Neugebauer, R., "Phase reflection – a new solution for the detection of shape defects on car body sheets", *Optical Engineering,* Vol 39(1), January 2000.

[12] Malacara, Daniel, 1992, *Optical Shop Testing*, John Wiley & Sons, Inc., New York.

[13] Bothe, T., Li, W., von Kopylow, C., Jüptner, W., 2004,"High Resolution 3D Shape Measurement on Specular Surfaces by Fringe Reflection", *Optical Metrology in Production Engineering*, Proceedings of SPIE Vol. 5457, Bellingham, WA.

[14] Burke, J., Bothe, T., Osten, W., Hess,C., 2002, "Reverse Engineering by Fringe Projection", *Proceedings of SPIE, vol 4778*, Bellingham, WA.

[15] Saldner, H.O., Huntley, J.M., 1997, "Profilometry Using Temporal Phase Unwrapping and a Spatial Light Modulator-Based Fringe Projector", *Optical Engineering,* vol 36(2), pp 610-615, Society of Photo-Optical Instrumentation Engineers.

[16] 2007, *Basler A641f Camera Specification*, Basler Vision Technologies Document #BD000410, Exton, PA.

[17] *Fujinon fixed focal length lenses,* www.fujinon.co.jp/en/products/cctv/pdf/h_2.pdf

[18] Bouguet, J-Y., 2008, "Camera Calibration Toolbox for Matlab", http://www.vision.caltech.edu/bouguetj/calib_doc/.

[19] *Disto Classic5 hand-held laser meter User manual,* Lieca Geosystems AG, Switzerland.

[20] Diver, R.B., and Andraka, C.E., 2003, "Integration of the Advanced Dish Development System", SAND2003-0780C, *International Solar Energy Conference Proceedings*, Kohala Coast, Hawaii Island, HI, March 15-18.

[21] Lopez, C. W. and Stone, K. W., "Design and Performance of the Southern California Edison Stirling Dish", *ASME J. of Solar Energy*, Vol. 2, pp. 945-952.

[22] Andraka, C.E. and Powell, M.P., "Dish Stirling Development For Utility-Scale Commercialization", *14th Biennial CSP SolarPACES Symposium*, Las Vegas NV, March 4-7, 2008.

[23] Andraka C.E., Diver R.B., Rawlinson K.S., "Improved Alignment Technique for Dish Concentrators" , SAND2003-0258C, Proceedings of ISEC 2003: 2003 International Solar Energy Conference , Mar 15,2003.

[24] Romero V. J., 1991, "CIRCE2/DEKGEN2: A Software Package for Facilitated Optical Analysis of 3-D Distributed Solar Energy Concentrators – Theory and User Manual," SAND91-2238, Sandia National Laboratories, Albuquerque, NM.